

Convective-diffusive transport in mercurous chloride (Hg_2Cl_2) crystal growth

Geug-Tae Kim*

Department of Nano-Bio Chemical Engineering, Hannam University, 133 Ojung-Dong, Daejeon 306-791, Korea

The effects of convection on the crystal growth rates of mercurous chloride (Hg_2Cl_2) are investigated for convective-diffusive conditions and purely diffusion conditions achievable in low gravity environments under a nonlinear thermal profile. For $4 \leq M_B \leq 472.086$, the solute driven convection (solulal Grashof number $Gr_s = 1.72 \times 10^5$) due to the disparity in the molecular weights of the component A (Hg_2Cl_2) and B (argon:Ar) is stronger than the thermally-driven convection (thermal Grashof number $Gr_t = 1.05 \times 10^4$), for an aspect ratio (transport length-to-width) of 5, total pressure of 35,455 Pascal, $Pr = 0.667$, $Le = 0.47$, $Pe = 3.57$, $C_v = 1.029$. With the temperature humps, there were found to be in undersaturations along the transport path for convective-diffusive processes ranging from $D_{AB} = 0.0584 \text{ cm}^2/\text{s}$ to $0.584 \text{ cm}^2/\text{s}$, in axial positions from 0 to 7.5 cm. The diffusion mode is predominant over convection for gravity levels less than $0.1 g_0$ for the horizontally-oriented configuration.

Key words: mercurous chloride, solute driven convection, physical vapor transport.

Introduction

Interest in growing mercurous chloride (Hg_2Cl_2) single crystals stems from their exceptional optical broad transmission range from 0.36 to 20 μm for applications in acousto-optic and opto-electronic devices such as Bragg cells, X-ray detectors operating at ambient temperature [1]. The equimolar Hg_2Cl_2 compound decomposes to two liquids at a temperature near 525 $^\circ\text{C}$ where the vapor pressure is well above 20 atmospheres [2, 3]. Because of this decomposition and high vapor pressure, Hg_2Cl_2 cannot be solidified as a single crystal directly from the stoichiometric melt. However, very similar to tmercurous bromide, mercurous chloride exhibits a sufficiently high vapor pressure at low temperatures so that these crystals are usually grown by the physical vapor transport (PVT) in closed silica glass ampoules. The PVT process has many advantages over melt-growth methods since it can be conducted at low temperatures: (1) vapor-solid interfaces possess relatively high interfacial/morphological stability against non-uniformities in heat and mass transfer; (2) high purity crystals are achieved; (3) materials decomposed before melting, such as Hg_2Cl_2 can be grown; (4) lower point defect and dislocation densities are achieved [4]. The mechanism of the PVT process is simple: sublimation-condensation in closed silica glass ampoules in a temperature gradient imposed between the source material and the growing crystal. In the PVT system for Hg_2Cl_2 , the molecular species Hg_2Cl_2 sublimates as the vapor phase from the crystalline source material

(Hg_2Cl_2), and is subsequently transported and re-incorporated into the single crystalline phase (Hg_2Cl_2) [5]. Recently PVT has become an important crystal growth process for a variety of acousto-optic materials. However, the industrial applications of the PVT process remain limited. One of important main reasons is that transport phenomena occurring in the vapor are complex and coupled so that it is difficult to design or control the process accurately. Such complexity and coupling are associated with the inevitable occurrence of thermal and/or solute driven convection generated by the interaction of gravity with density gradients arising from temperature and/or concentration gradients. In general, convection has been regarded as detrimental and, thus, to be avoided or minimized in PVT growth system. These thermal/and/or solute driven convection-induced complications result in problems ranging from crystal inhomogeneity to structural imperfections. Therefore, in order to analyze and control the PVT process accurately, and also make significant improvements in the process, it is essential to investigate the roles of convection in the PVT process.

Markham *et al.* [6] examined the effects of thermal and thermosolutal convections during the PVT process inside vertical cylindrical enclosures for a time-independent system, and showed that even in the absence of gravity, convection can be present, causing nonuniform concentration gradients. They emphasized the role of geometry in the analysis of the effects of convection. As such these fundamentally constitute steady state two-dimensional models. The steady state models are limited to low Rayleigh number applications, because as the Rayleigh number increases oscillation of the flow field occurs. To address the issue of unsteady flows in PVT, Duval [7] performed a numerical study

*Corresponding author:
Tel : +82-42-629-7984
Fax: +82-42-623-9489
E-mail: gtkim@hannam.ac.kr

on transient thermal convection in the PVT processing of Hg_2Cl_2 very similar to the mercurous bromide for a vertical rectangular enclosure with insulated temperature boundary conditions for Rayleigh numbers up to 10^6 . Nadarajah *et al.* [8] addressed the effects of solutal convection for any significant disparity in the molecular weights of the crystal components and the inert gas. Zhou *et al.* [9] reported that the traditional approach of calculating the mass flux assuming one-dimensional flow for low vapor pressure systems is indeed correct. Rosenberger *et al.* [10] studied three-dimensional numerical modeling of the PVT process which yielded quantitative agreement with measured transport rates of iodine through octofluorocyclobutane (C_4F_8) as inert background gas in horizontal cylindrical ampoules.

In this theoretical study, a two-dimensional model is used for the analysis of the PVT processes during vapor-growth of mercurous chloride crystals (Hg_2Cl_2) in horizontally oriented, cylindrical, closed ampoules in a two-zone furnace system. Diffusion-limited processes are considered in this paper, although the recent paper of Singh *et al.* [11] demonstrated that the interfacial kinetics plays an important role in the PVT system of Hg_2Cl_2 . Thermo-solutal convection will be considered at this point, primarily because a mixture of Hg_2Cl_2 vapor and impurity of argon (Ar) is used. Thermal convection can be ignored in comparison to solutally-induced convection for the imposed nonlinear thermal profile to prevent supersaturation along the transport path.

It is the purpose of this paper (1) to relate the applied convective process parameters such as gravitational acceleration perturbations, molecular weight of an inert gas and the partial pressure of an inert gas to the crystal growth and its distribution across an interface (2) to examine the effects of solute driven convection with a nonlinear temperature profile in order to gain insights into the underlying physicochemical processes.

The model

Consider a rectangular enclosure of height H and transport length L , shown in Fig. 1. The source is maintained at a temperature T_s , while the growing crystal is at a temperature T_c , with $T_s > T_c$. The PVT of the transported component A (Hg_2Cl_2) occurs inevitably, due to the presence of impurities, with the presence of an inert component B (Ar). The interfaces are assumed to be flat for simplicity. The finite normal velocities at the interfaces can be expressed by Stefan flow deduced from the one-dimensional diffusion-limited model [12], which would provide the coupling between the fluid dynamics and species calculations. On the other hand, the tangential component of the mass average velocity of the vapor at the interfaces vanishes. Thermodynamic equilibria are assumed at the interfaces so that the mass

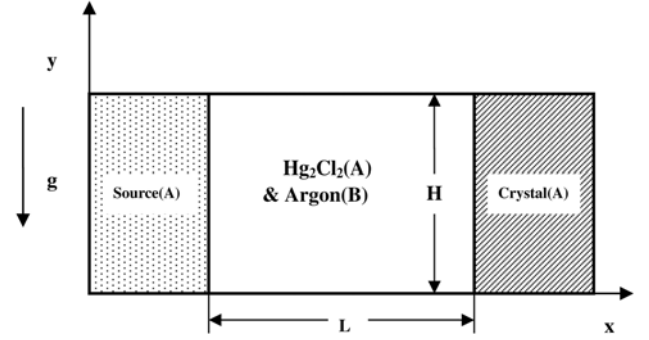


Fig. 1. Schematic of PVT growth reactor in a two-dimensional rectangular system.

fractions at the interfaces are kept constant at $\omega_{A,s}$ and $\omega_{A,c}$. On the vertical non-reacting walls appropriate velocity boundary conditions are no-slip, the normal concentration gradients are zero, and wall temperatures are imposed as nonlinear temperature gradients.

Thermophysical properties of the fluid are assumed to be constant, except for the density. When the Boussinesq approximation is invoked, density is assumed constant except for the buoyancy body force term. The density is assumed to be a function of both the temperature and concentration. The ideal gas law and Dalton's law of partial pressures are used. Viscous energy dissipation and the Soret-Dufour (thermo-diffusion) effects can be neglected, as their contributions remain relatively insignificant for the conditions encountered in our PVT crystal growth processes. Radiative heat transfer can be neglected under our conditions, based on Kassemi and Duval [13].

The transport of fluid within a rectangular PVT crystal growth reactor is governed by a system of elliptic, coupled conservation equations for mass (continuity), momentum, energy and species (diffusion) with their appropriate boundary conditions. Let v_x , v_y denote the velocity components along the x - and y -coordinates in the x , y rectangular coordinate system, and let T , ω_A , p denote the temperature, mass fraction of species A (Hg_2Cl_2) and pressure, respectively.

The dimensionless variables are scaled as follows:

$$x^* = \frac{x}{H}, y^* = \frac{y}{H} \quad (1)$$

$$u = \frac{u_x}{U_c}, v = \frac{v_y}{U_c}, p = \frac{p}{\rho_c U_c^2} \quad (2)$$

$$T^* = \frac{T - T_c}{T_s - T_c}, \omega_A^* = \frac{\omega_A - \omega_{A,c}}{\omega_{A,s} - \omega_{A,c}} \quad (3)$$

The dimensionless governing equations are given by:

$$\nabla^* \cdot \vec{V}^* = 0, \quad (4)$$

$$\vec{\nabla}^* \cdot \nabla^* \vec{V}^* = -\nabla^* p^* + Pr \nabla^{*2} \vec{V}^* - Ra \cdot Pr \cdot T^* \cdot \vec{e}_g, \quad (5)$$

$$\vec{V}^* \bullet \nabla^* T^* = \nabla^{*2} T^* \quad (6)$$

$$\vec{V}^* \bullet \nabla^* \omega_A^* = \frac{1}{Le} \nabla^{*2} \omega_A^* \quad (7)$$

These nonlinear, coupled sets of equations are numerically integrated with the following boundary conditions:

On the walls ($0 < x^* < L/H$, $y^*=0$ and 1):

$$u(x^*, 0) = u(x^*, 1) = v(x^*, 0) = v(x^*, 1) = 0 \quad (8)$$

$$\frac{\partial \omega_A^*(x^*, 0)}{\partial y^*} = \frac{\partial \omega_A^*(x^*, 1)}{\partial y^*} = 0,$$

$$T^*(x^*, 0) = T^*(x^*, 1) = \frac{T_s - T_c}{T_s - T_c}$$

On the source ($x^*=0$, $0 < y^* < 1$):

$$u(0, y^*) = -\frac{1}{Le(1-\omega_{A,s})} \frac{\partial \omega_A^*(0, y^*)}{\partial x^*}, \quad (9)$$

$$v(0, y^*) = 0,$$

$$T^*(0, y^*) = 1,$$

$$\omega_A^*(0, y^*) = 1.$$

On the crystal ($x^*=L/H$, $0 < y^* < 1$):

$$u(L/H, y^*) = -\frac{1}{Le(1-\omega_{A,c})} \frac{\partial \omega_A^*(L/H, y^*)}{\partial x^*} \quad (10)$$

$$v(L/H, y^*) = 0,$$

$$T^*(L/H, y^*) = 0,$$

$$\omega_A^*(L/H, y^*) = 0.$$

The following temperature profile was used as a boundary condition along the ampoule ($y=0$ and $y=H$): this equation is expressed with reference to an approximate fit of experimental data [14, 15], see Fig. 2.

$$T(t) = \begin{cases} 563.16 & \text{for } -20 \leq t \leq -10 \text{ cm} \\ 608 + 4.97t - 0.70t^2 - 5.91 \times 10^{-2}t^3 + 6.67 \times 10^{-3}t^4 \\ + 2.60 \times 10^{-4}t^5 - 2.49 \times 10^{-5}t^6 & \text{for } -10 \leq t \leq 12 \text{ cm} \\ 593.16 & \text{for } 12 \leq t \leq 20 \text{ cm} \end{cases} \quad (11)$$

Relative to Fig. 2, during the crystal growth the ampoule is placed in the nonlinear thermal profile as shown in Fig. 3. The hump region corresponds to the location of the vapor component of A and B inside the ampoule. The source material lies in the region with the larger temperature near $t \geq 8$ cm; whereas crystal growth occurs in the region corresponding to $t \leq -4$ cm. In our experiments one positions the ampoule in the

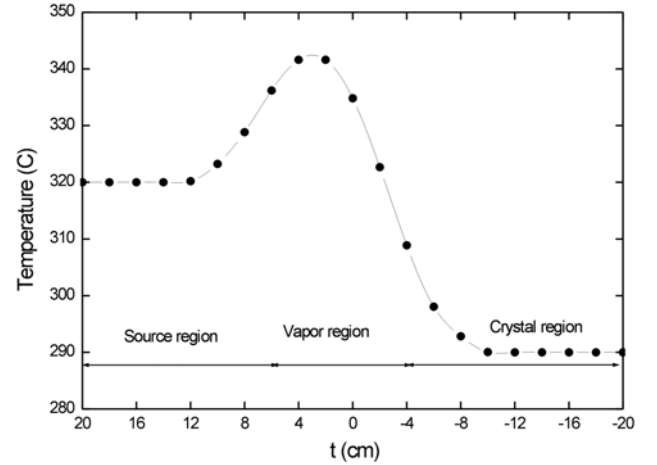


Fig. 2. The temperature profile along the ampoule [14].

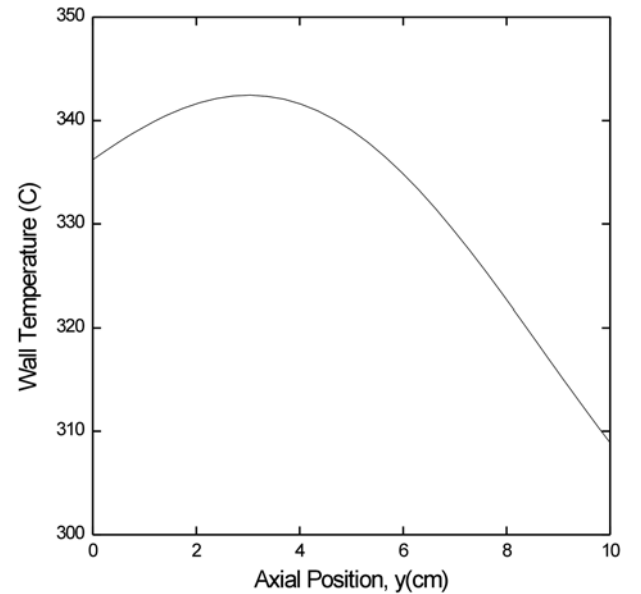


Fig. 3. An axial temperature profile given by Eq. (11) with maximum (“hump”) between T_s and T_c .

growth region with a temperature less than the source in order to drive the process. In addition, the length of the hump region can also be adjusted so that we have a much larger source region. With respect to Fig. 3, the following transformation is used to relate the laboratory reference system to that of the $x=K_i-t$ ampoule: where K_i is the position of the source and vapor interface in the laboratory reference frame.

In the dimensionless parameters in the governing equations the thermophysical properties of the gas mixture are estimated from gas kinetic theory using Chapman-Enskog's formulas [16].

The vapor pressure [17] p_A of Hg_2Cl_2 (in the unit of Pascal) can be evaluated from the following formula as a function of temperature: in which $a = 29.75$, $b = 11767.1$.

$$p_A = e^{(a-b/T)}, \quad (12)$$

The crystal growth rate V_c is calculated from a mass balance at the crystal vapor interface, assuming fast kinetics, i.e. all the vapor is incorporated into the crystal, which is given by (subscripts c, v refer to crystal and vapor respectively):

$$\int \rho_v v_v \cdot n dA = \int \rho_c v_c \cdot n dA, \quad (13)$$

$$v_c = \frac{\rho_v \int v_v \cdot n dA}{\rho_c \int dA}. \quad (14)$$

The detailed numerical schemes in order to solve the discretization equations for the system of nonlinear, coupled governing partial differential equations are found in [18].

Results and Discussion

The parametric study is useful for showing trends and generalizing the problem, but many parameters are involved in the problem under consideration, which renders it difficult for a general analysis. One of the purposes of this study is to correlate the growth rate and the interfacial distributions, and partial pressure of A (p_A) to process parameters such as molecular weight of B (M_B), gravity level, nonlinear and linear thermal profile, and binary diffusivity for a particular material (Hg_2Cl_2). Thus, it is desirable to express some results in terms of dimensional growth rate, however they are also applicable to parameter ranges over which the process varies in the manner given. The six dimensionless parameters, namely Gr , Ar , Pr , Le , C_v and Pe , are independent and arise naturally from the dimensionless governing equations and boundary conditions. The dimensionless parameters and physical properties for the operating conditions of this study are shown in

Table 1. Typical thermo-physical properties used in this study ($M_A = 472.086$, $M_B = 39.95$)

Transport length, L	10 cm
Height, H	2 cm
Source temperature, T_s	336.21 °C
Crystal temperature, T_c	308.89 °C
Density, ρ	0.002048 g/cm ³
Dynamic viscosity, μ	0.00029 g/(cm·sec)
Diffusivity, D_{AB}	0.584 cm ² /s
Thermal expansion coefficient, β	0.0017 K ⁻¹
Prandtl number, Pr	0.667
Lewis number, Le	0.47
Peclet, Pe	3.57
Concentration number, C_v	1.029
Total system pressure, P_T	35,455 Pascal
Thermal Grashof number, Gr_t	1.05×10^4
Solutal Grashof number, Gr_s	1.72×10^5

Table 1.

In this study, the effects of an inert component whose molecular weight is not equal to that of the crystal component during the physical vapor transport are considered. In this case $M_A \neq M_B$; both solute driven and thermal effects are considered. If solutal convection is dominant, the imposed temperature profile has little effect on the growth rate [8]. Conductive wall boundary conditions with a nonlinear thermal profile are considered, while the insulated walls are not considered because it is difficult to obtain in practice and most vapor growth experiments are performed under an imposed nonlinear thermal profile to avoid nucleation at the ampoule walls. Figure 3 shows the axial temperature profile given by Eq. (11) with a maximum (“hump”) between T_s and T_c . To prevent undesirable nucleation on the walls, an often used experimental technique is to impose a nonlinear thermal profile with a maximum between the crystal and the source, which is usually referred to as a temperature “hump”. This temperature hump could eliminate the problem of vapor supersaturation along the transport path and, thus, of parasitic nucleation on the walls. But, these humps may result in sharp temperature gradients near the crystal region, inducing thermal stresses and a decrease in crystal quality. A temperature hump of 27 K with $T_s = 336$ °C, $T_c = 309$ °C is selected for this study.

In Fig. 4 the equilibrium vapor transport pressure profile is obtained from Eq. (12) for the hump thermal profile shown in Fig. 3. The partial pressures of component A (Hg_2Cl_2) at the walls are gained from convective-diffusive transport at the horizontal orientation with $1g_0$ and Ar (aspect ratio: transport length-to-

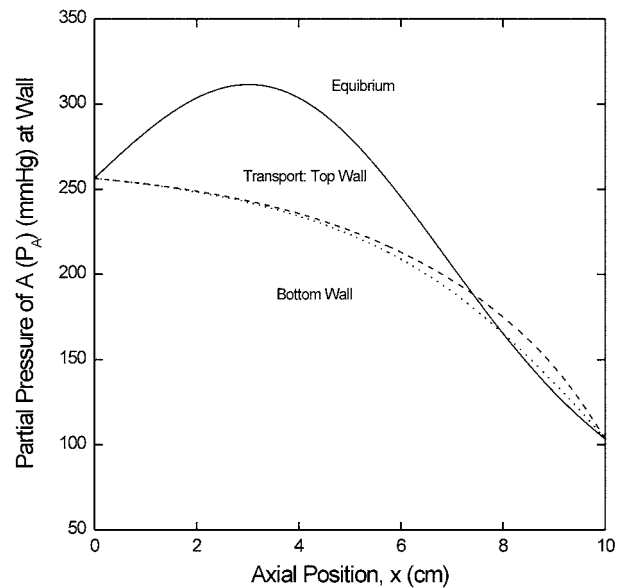


Fig. 4. An axial distribution of partial pressures of component A at the walls resulting from diffusive-convective transport at $g_y=1g_0$, and equilibrium vapor transport pressure, for $Ar (L/H)=5$ and the nonlinear wall temperature profile of Fig. 3.

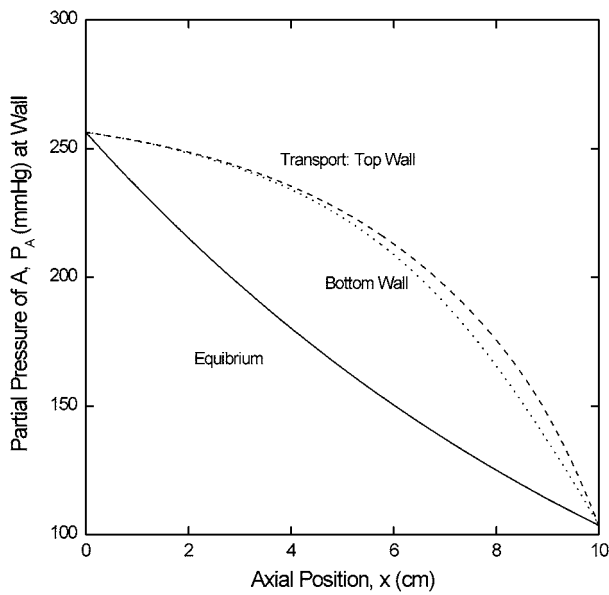


Fig. 5. An axial distribution of partial pressures of component A at the walls resulting from diffusive-convective transport at $g_y=1g_0$, and equilibrium vapor transport pressures, for $Ar(L/H)=5$ and the linear wall temperature profile.

width) of 5. It is clear that the hump thermal profile is necessary to prevent nucleation on the walls and the elimination of supersaturation along the transport path. For $7.5 \leq x \leq 10$ cm, the supersaturation of vapor A (Hg_2Cl_2) occurs due to wall temperatures lower than the temperatures at top and bottom walls inside an ampoule, which is directly related to the convective-diffusive flow pattern [8, 19], not shown here. Therefore, to avoid the parasitic nucleation of the component A near the crystal region, a larger hump profile near the crystal would be necessary, which is realistic in experiments. The higher concentration along the top wall reflects the clockwise sense of rotation of the solute driven convection.

Figure 5 shows that with a linear temperature profile, the vapor of component A (Hg_2Cl_2) is supersaturated throughout the ampoule. It is clear to see why a linear temperature profile is rarely used in practice. Figure 6 shows the axial distribution of partial pressures of component A for a system with the same conditions as for Fig. 4 with $D_{AB}=0.584$ cm^2/s , except for a binary diffusion coefficient of 0.0584 cm^2/s . The much smaller value of the diffusion coefficient can be obtained with inert gases of larger molecular weight or hydrogen pairs at higher total pressure. In this study, instead of using either inert gases with a larger molecule weight or the hydrogen pairs, the diffusion coefficient of 0.584 cm^2/s in Fig. 4 is intentionally decreased by a factor of an one-tenth and reduced to 0.0584 cm^2/s in Fig. 6 for the study of the effects of diffusion transport on the axial distribution of partial pressures of component A (Hg_2Cl_2). As shown in Fig. 6, with lower diffusion coefficients, a convection mode is predominant over a

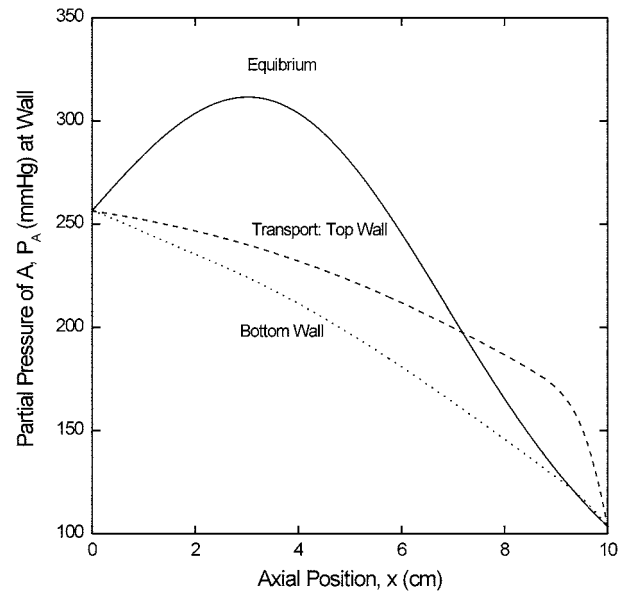


Fig. 6. An axial distribution of partial pressures of component A (Hg_2Cl_2) for system as in Fig. 4 except for $D_{AB}=0.0584$ cm^2/s .

diffusion mode because of greater diffusion limitation so that the occurrence of supersaturation near the crystal region would arise, reflecting a relatively small hump profile of the partial pressure of A. Fig. 6 shows a remarkable difference in partial pressure of A between the top and bottom walls in a comparison with Fig. 4. This is due to the effects of diffusion-limited convection near the crystal region. As discussed later, under lower gravity environments, the diffusion dominates so that a smaller hump thermal profile would be quite appropriate for suppressing the parasitic nucleation near the crystal. The temperature dependence of the diffusivity on the nonlinear thermal profile is reflected through a binary diffusion coefficient as a function of temperature, which can be calculated from Chapman-Enskog's formula [16]. But, the effect of nonlinear temperature humps would be negligible because of the small temperature difference employed.

Figure 7 shows the interfacial distributions of crystal growth rates of Hg_2Cl_2 for two different gravity levels of $g_y = 1g_0$ and $0.1g_0$. One sees that convection causes significant nonuniformity near the growing crystals so that it would have a profound influence on the qualities and morphologies of the crystal. The extent of nonuniformity (σ) of the growth rate is defined as:

$$\sigma(\%) = \frac{V_{c,max} - V_{c,min}}{V_c} \times 100$$

in which $V_{c,max}$ is the local maximum growth rate, $V_{c,min}$ is the local minimum growth rate, and V_c is the average growth rate across the crystal surface. The nonuniformity (σ) here can be considered as the relative magnitude of the local Hg_2Cl_2 vapor velocity according to the mass flux balances [19]. The nonuniformity (σ) of the earth is 34.75%, while that of $0.1g_0$ is 9.54%.

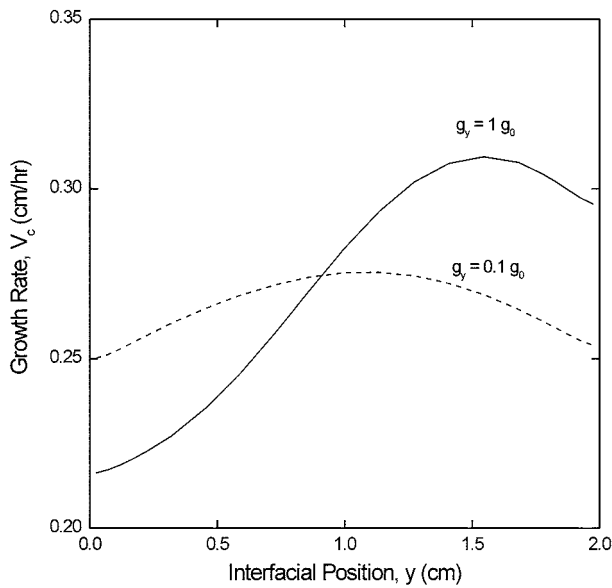


Fig. 7. Interfacial distribution of crystal growth rates of Hg_2Cl_2 for the nonlinear conducting walls with an aspect ratio (L/H) of 5 and the horizontal orientation, $g_y = 1g_0, 0.1g_0$.

The former is greater than the latter by a factor of 3.64, indicative of the intensity of convection. The convection causes significant nonuniformities in the growth rate across the interface in the crystal region, which is consistent with the results of Markham *et al.* [6]. From the viewpoint of the growth rate profile, the rate profile for $0.1g_0$ is symmetrical across the crystal interfaces, where the diffusion mode is expected to be predominant over the convection mode. For $0.1g_0$, the growth rate profile has a parabolic pattern, which indicates that the Stefan wind suppresses the convection mode. The parabolic pattern of the growth rate distributions indicates the flow field is controlled by diffusion, as not shown here [8]. Discussions over these predictions remain for future studies. The growth rate profiles for $1g_0$ are asymmetrical across the interface, which reflects the occurrence of more than one convective cell near the crystal region. Therefore, as the intensity of convection increases, the extent of nonuniformity increases as well as the symmetrical extent.

One now investigates the effects of the molecular weight of component B, M_B on the growth rate and interfacial distributions across the crystal. Fig. 8 illustrates the molecular weight of B dependence of the growth rates and interfacial distributions for $4 \leq M_B \leq 472.086$. It can be seen that the nonuniformities and the growth rate profiles are nearly the same for all interfacial positions across the crystal. All the rate profiles are asymmetrical with respect to the central interfacial position ($y = 1.0$ cm). The position of maximum growth rate for $M_B = 4.0$ is at nearly $y = 1.25$ cm and the positions for other weights are placed around $y = 1.5$ cm. As the weight of B is decreased, the rate is increased. Below the value of 28 (corresponding to

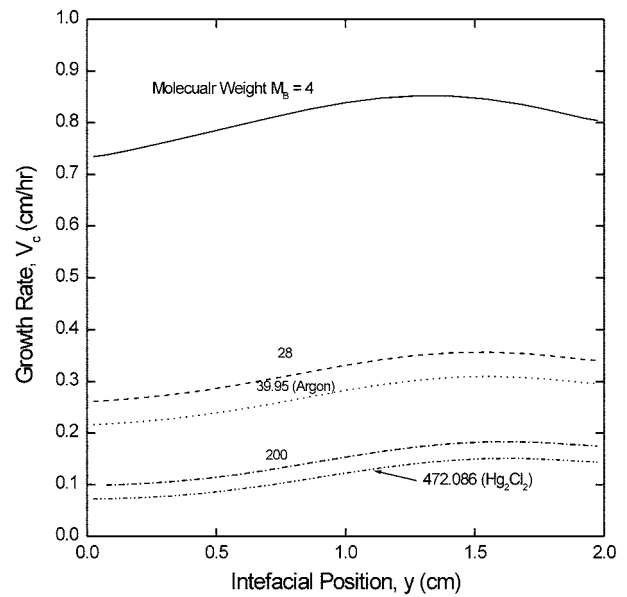


Fig. 8. Effects of molecular weight M_B on interfacial distribution of crystal growth rates of Hg_2Cl_2 for the nonlinear thermal profile with an aspect ratio of 5.

N_2), the rate sharply increases with the weight of B. When M_B is reduced by a factor of 9.99, i.e., 39.95 to 4, the maximum rate is increased by a factor of 2.75: for $M_B = 39.95$, $V_c = 0.309$ cm/h, $M_B = 4$, $V_c = 0.852$ cm/h. On the other hand, when M_B is enlarged by a factor of 11.9, i.e., 39.95 to 472.086, the maximum rate is decreased by a factor of 2.05: for $M_B = 39.95$, $V_c = 0.309$ cm/h; $M_B = 4$, $V_c = 0.150$ cm/h. Note that the case of $M_B = 472.086$ corresponds to a self-diffusion system which is encountered with highly purified materials: $M_B = 4$ corresponds to helium (He); $M_B = 28$ corresponds to nitrogen (N_2). Because the molecular weight of component B is set to be same as that of component A, only thermal convection is considered and the effect of solute driven convection arising owing to concentration gradients is neglected. In other words, when thermal convection is dominant, i.e., $M_A = M_B$ at $1g_0$. The effect of thermal convection is reflected through the density term and the binary diffusivity coefficient by setting $M_A = M_B$. Figure 9 shows the dependence of M_B on the growth rate for $4 \leq M_B \leq 472.086$. As one sees in Fig. 9, the rate decreases exponentially with M_B for $Ar = 5$, $H = 2$ cm, $T_s = 336.21$ °C, $T_c = 308.89$ °C. In Fig. 9, a linear scale is chosen to demonstrate the functional relationship of the rate to the molecular weight of component B, M_B . As pointed out previously, it is understood in Fig. 9 that in the present study solute driven convection dominates over thermal convection because the rate for $M_B = 472.086$ corresponding to the case of thermal convection is smaller than that for $M_B (\neq M_A)$. Note that in Figs. 8 and 9, the effect of the molecular weight of B is reflected only through the binary diffusivity and not through the density term, which would not have a

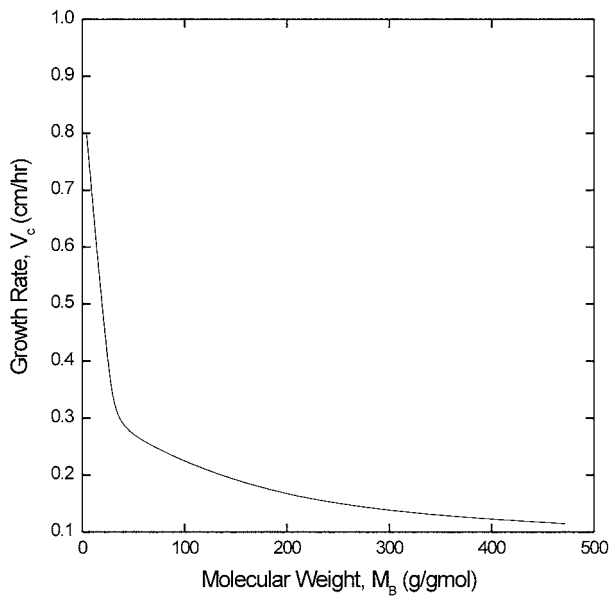


Fig. 9. Influence of molecular weight M_B on crystal growth rates of Hg_2Cl_2 , which corresponds to Fig. 8.

profound effect on the intensity of solute driven convection. It should also be emphasized that even if the driving force of solutally driven convection (solute driven convection) contains both temperature and concentration gradients, it is impossible to isolate solute driven convection completely from thermo-solutal convection because the PVT method is based on the driving force of a temperature gradient.

Figure 10 shows the effects of gravitational acceleration on the crystal growth rates. Levels of gravity acceleration ranging between $10^{-5}g_0$ and $1g_0$ are considered for the positive y -direction (horizontal configuration), where g_0 denotes the standard gravitational

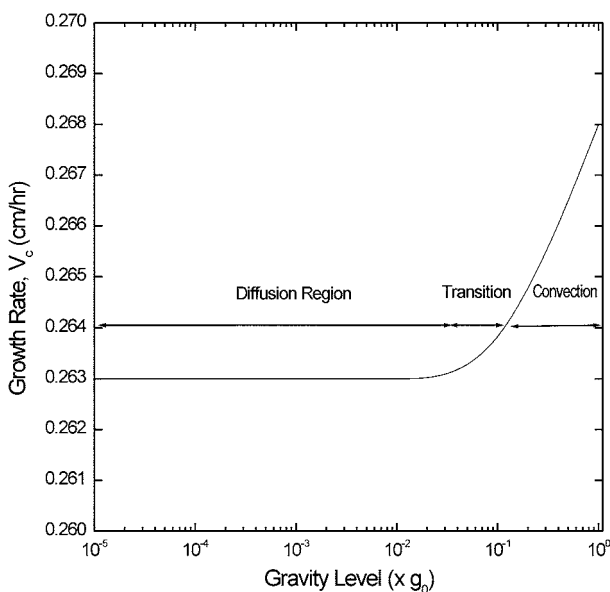


Fig. 10. Growth rates of Hg_2Cl_2 as a function of the gravity level, $10^{-5}g_0 \leq g_y \leq 1g_0$.

acceleration constant, 980.665 cm/s^2 . For $g_y = 1g_0$, the corresponding dimensionless parameters are thermal Grashof number $Gr_t = 1.05 \times 10^4$, solutal Grashof number $Gr_s = 1.72 \times 10^5$, $Ar = 5$, $Pr = 0.667$, $Le = 0.47$, $Pe = 3.57$, $C_v = 1.029$ and the total pressure of 35,455 Pascal. The growth rate is sharply decreased by a ten times reduction of gravitational acceleration. Two distinct regions are shown: convection and diffusion regions. For microgravity environments less than $0.1g_0$, the rate exhibits a relatively flat profile, because the transport is a diffusive mode. For the levels below $0.1g_0$, no recirculating cell is present. Above $10^{-1}g_0$, the flow switches to convective mode, and a recirculating cell is expected to appear in the vapor phase, referring to Figs. 6 and 7. Therefore, the study of convection under the microgravity environments provides an important insight of understanding the essence of convection. For gravity levels less than $10^{-1}g_0$, the diffusion mode is dominant so that the Stefan wind drives the flow. Note that in a low gravity environment the growth rates could be changed by using smaller aspect ratio ampoules or larger temperature differences between source and the crystal, without the drawback of increased convection which would occur on ground-experiments [8, 21]. Therefore, no recirculating cell is predicted for the operating conditions under consideration.

Conclusions

It is concluded that for $4 \leq M_B \leq 472.086$, the solute driven convection ($Gr_s = 1.72 \times 10^5$) due to the disparity in the molecular weights of the component A (Hg_2Cl_2) and B (Ar) is stronger than the thermally driven convection ($Gr_t = 1.05 \times 10^4$), for an aspect ratio (transport length-to-width) of 5, total pressure of 35,455 Pascal, $Pr = 0.667$, $Le = 0.47$, $Pe = 3.57$, $C_v = 1.029$. A temperature hump is found to be most efficient in suppressing parasitic nucleation. With a temperature hump, undersaturations along the transport path were found for convective-diffusive processes ranging from $D_{AB} = 0.0584 \text{ cm}^2/\text{s}$ to $0.584 \text{ cm}^2/\text{s}$, axial positions from 0 to 7.5 cm. The diffusion mode is predominant over the convection mode for gravity levels less than $0.1g_0$ for the horizontally oriented configuration, $Gr_t = 1.05 \times 10^4$, $Gr_s = 1.72 \times 10^5$, $Ar = 5$, $Pr = 0.667$, $Le = 0.47$, $Pe = 3.57$, $C_v = 1.029$ and $P_T = 35,455$ Pascal.

References

1. N.B. Singh, M. Gottlieb, G.B. Brandt, A.M. Stewart, R. Mazelsky, and M.E. Glicksman, *J. Crystal Growth* 137 (1994) 155-160.
2. N.B. Singh, R.H. Hopkins, R. Mazelsky, and J.J. Conroy, *J. Crystal Growth* 75 (1970) 173-180.
3. S.J. Yosim and S.W. Mayer, *J. Phys. Chem.* 60 (1960) 909-911.
4. F. Rosenberger, *PhysicoChemical Hydrodynamics* 1 (1980)

- 3-26.
5. N.B. Singh, M. Gottlieb, A.P. Goutzoulis, R.H. Hopkins, and R. Mazelsky, *J. Crystal Growth* 89 (1988) 527-530.
6. B.L. Markham, D.W. Greenwell and F. Rosenberger, *J. Crystal Growth* 51 (1981) 426-437.
7. W.M.B. Duval, *J. Chemical Vapor Deposition* 2 (1994) 188-217.
8. A. Nadarajah, F. Rosenberger, and J. Alexander, *J. Crystal Growth* 118 (1992) 49-59.
9. H. Zhou, A. Zebib, S. Trivedi, and W.M.B. Duval, *J. Crystal Growth* 167 (1996) 534-542.
10. F. Rosenberger, J. Ouazzani, I. Viohl, and N. Buchan, *J. Crystal Growth* 171 (1997) 270-287.
11. N.B. Singh, R. Mazelsky, and M.E. Glicksman, *Physico Chemical Hydrodynamics* 11 (1989) 41-48.
12. F. Rosenberger and G. Müller, *J. Crystal Growth* 65 (1983) 91-104.
13. M. Kassemi and W.M.B. Duval, *J. Thermophys. Heat Transfer* 4 (1989) 454-461.
14. N.B. Singh and W.M.B. Duval, NASA Technical Memorandum 103788 (1991).
15. C. Mennetrier, W.M.B. Duval, and N.B. Singh, NASA Technical Memorandum 105920 (1992).
16. R.B. Bird, W.E. Stewart, and E.N. Lightfoot, in "Transport Phenomena" (New York, NY: John Wiley and Sons, 1960).
17. C. Mennetrier and W.M.B. Duval, NASA Technical Memorandum 105371(1991).
18. S.V. Patankar, in "Numerical Heat Transfer and Fluid flow" (New York, NY: McGraw-Hill, 1980).
19. G.T. Kim, W.M.B. Duval, M.E. Glicksman, and N.B. Singh, *Modelling simu. Mater. Sci. Eng.* 3 (1995) 331-357.
20. I. Catton, *J. Heat Transfer* 94 (1972) 446-452.
21. G.T. Kim and M.H. Kwon, *J. Korean Crystal Growth and Crystal Technology* 14 (2004) 160-168.